[8]Moetakef, M. A., Joshi, S. P., and Lawrence, K. L., "Finite Element Simulation of Bulk Elastic Waves in Piezceramic Transducers Using Interdigital Electrodes," *Proceedings of the SPIE*, Vol. 2442, International Society of Optical Engineering, Bellingham, WA, 1995, pp. 182–187.

[9]Hofer, B., "Fibre Optic Damage Detection in Composite Structures," *Composites*, Vol. 17, No. 4, 1987, pp. 309–316.

[10]Waite, S. R., Tatam, R. P., and Jackson, A., "Use of Optical Fibre for Damage and Strain Detection in Composite Materials," *Composites*, Vol. 19, No. 6, 1988, pp. 435–442.

[11]Salawu, O. S., "Detection of Structural Damage Through Changes in Frequency: A Review," *Engineering Structures*, Vol. 19, No. 9, 1997, pp. 718–723.

[12]Tsai, W. H., and Yang, J. C. S., "Nondestructive Evaluations of Composite Structures Using System Identification Technique," *Journal of Engineering Materials and Technology*, Vol. 110, No. 2, 1988, pp. 134–139.

[13]Lew, J. S., "Using Transfer Parameter Changes for Damage Detection of Structures," *AIAA Journal*, Vol. 33, No. 11, 1995, pp. 2189–2193.

[14]Jian, X. H., Tzou, H. S., and Penn, L. S., "Damage Detection in by Piezoelectric Patches in a Free Vibration Method," *Journal of Composite Materials*, Vol. 31, No. 4, 1997, pp. 345–359.

[15]Valentin, D., and Busell, A. R., "Damage Detection in Carbon Fibre Epoxy Composites," *Composite Structures 2: Proceedings of 2nd International Conference*, Applied Science Publications, London, 1983, pp. 40–52.

[16]Sun, F. P., Chaudhry, Z., Liang, C., and Rogers, C. A., "Truss Structure Integrity Identification Using PZT Sensor–Actuator," *Journal of Intelligent Material Systems and Structures*, Vol. 6, No. 1, 1995, pp. 134–139.

[17]Ayres, J. W., Lalande, F., Chaudhry, Z., and Rogers, C. A., "Qualitative Impedance-Based Health Monitoring of Civil Infrastructures," *Smart Materials and Structures*, Vol. 7, No. 5, 1998, pp. 599–605.

[18]Liang, C., Sun, F. P., and Rogers, C. A., "Dynamic Analysis of Active Material Systems," *Journal of Vibration and Acoustics*, Vol. 116, No. 1, 1994, pp. 120–128.

[19]Vipperman, J. S., and Clark, R. L., "Implementation of an Adaptive Piezoelectric Sensoriactuator," *AIAA Journal*, Vol. 34, No. 10, 1996, pp. 2102–2109.

[20]Vipperman, J. S., and Clark, R. L., "Multivariable Feedback Active Structural Acoustic Control Using Piezoelectric Sensoriactuators," *Journal of the Acoustical Society of America*, Vol. 105, No. 1, 1999, pp. 219–225.

[21]Vipperman, J. S., and Clark, R. L., "Hybrid Analog and Digital Adaptive Compensation of Piezoelectric Sensoriactuators," *Proceedings of the AIAA/ASME/ASCE/AHS/ASC Structures, Structural Dynamics, and Materials Conference*, AIAA, Washington, DC, 1995, pp. 2854–2859.

[22]Board, I. S., *IEEE Standard on Piezoelectricity*, Inst. of Electrical and Electronics Engineers, New York, 1988, Sec. 2.

[23]Cady, W., *Piezoelectricity: An Introduction to the Theory and Applications of Electromechanical Phenomena in Crystals*, 2nd ed., Dover, New York, 1964, Chap. 8.

[24]Bunget, I., *Physics of Solid Dielectrics*, Elsevier, New York, 1984.

[25]Kinsler, L. E., Frey, A. R., Coppens, A. B., and Sanders, J. V., *Fundamentals of Acoustics*, 3rd ed., Wiley, New York, 1982.

[26]Jaffe, B., Cook, W., and Jaffe, H., *Piezoelectric Ceramics*, Academic Press, New York, 1971, Chap. 2.

[27]Dosch, J. J., Inman, D. J., and Garcia, E., "A Self-Sensing Piezoelectric Actuator for Collocated Control," *Journal of Intelligent Material Systems and Structures*, Vol. 3, Jan. 1992, pp. 166–185.

[28]Hagood, N. W., and Anderson, E. H., "Simultaneous Sensing and Actuation Using Piezoelectric Materials," *Active and Adaptive Optical Components*, SPIE Vol. 1453, International Society for Optical Engineering, Bellingham, WA, 1991, pp. 409–421.

[29]Cole, D. G., and Clark, R. L., "Adaptive Compensation of Piezoelectric Sensoriactuators," *Journal of Intelligent Material Systems and Structures*, Vol. 5, Sept. 1994, pp. 665–672.

[30]Vipperman, J. S., "Adaptive Piezoelectric Sensoriactuators for Active Structural Acoustic Control," Ph.D. Dissertation, Dept. of Mechanical Engineering, Duke Univ., Durham, NC, Feb. 1997.

[31]Oppenheim, A. V., and Schafer, R. W., *Digital Signal Processing*, Prentice–Hall, Englewood Cliffs, NJ, 1975.

[32]Vipperman, J. S., and Li, D., "Dielectric Response of Adaptive Piezoelectric Sensoriactuators," American Society of Mechanical Engineers, *International Mechanical Engineering Congress and Exposition Proceedings*, Nov. 2000.

A. M. Baz
*Associate Editor*

# Experimental Validation of Nonlinear Shell Structural Dynamics

Daniel Berggren*
*Royal Institute of Technology,*
*SE-100 44 Stockholm, Sweden*

## Introduction

In recent years there has been an increased interest in nonlinear aeroelasticity. Phenomena such as limit-cycle oscillations (LCOs) have been observed in flight testing,[1,2] but the cause of the LCOs is not yet fully understood. Most researchers agree that the limit cycles are an effect of nonlinearities in the fluid-structure interaction. However, it is not always obvious whether the dominant nonlinearities are caused by structural nonlinearities or aerodynamic nonlinearities.

Methods for analysis of LCOs have been developed by, for example, Patil et al.[3] and Tang et al.[4] with some success. The former models the wing using beam theory and the latter a method based on the von Kármán plate equations. The structural dynamic analysis can be improved using nonlinear shell finite elements for the wing. This is a well-established model[5,6] for structural dynamics analysis but has not yet been used much for analysis of nonlinear aeroelasticity.

The long term goal of the author's research is to investigate LCOs for a cantilever wing configuration using nonlinear shell finite elements combined with aerodynamic forces based on a linear unsteady potential flow model. However, there are not many test cases available in the open literature where experimental results are presented, making it possible to investigate the accuracy of the computational method. Because of this, experiments have been performed in the present study in order to investigate the accuracy of the structural dynamics model. In this Note a well-defined reference case is presented together with a brief description of the nonlinear analysis method used. The geometry, material properties, experimental results as well as computational results are given in order to make it possible to use the data as a reference case when developing methods for analysis of nonlinear structural dynamics.

## Governing Equations

The equations of motion for a shell structure modeled with finite elements[7] are given by

$$\boldsymbol{M}\ddot{\boldsymbol{a}} + \boldsymbol{F}_{\text{int}}(\boldsymbol{a}) = \boldsymbol{F}_{\text{ext}}(t, \boldsymbol{a}) \tag{1}$$

where $\boldsymbol{M}$ is the linear mass matrix, $\boldsymbol{F}_{\text{int}}$ is a vector of internal forces, $\boldsymbol{F}_{\text{ext}}$ is a vector of external forces, and $\boldsymbol{a} = \boldsymbol{a}(t)$ is the time-dependent nodal displacement vector. The implicit Newmark average acceleration time-stepping algorithm[7] was chosen to solve Eq. (1) numerically. In each time step a Newton iteration has to be performed, and therefore, in addition to the internal forces, the tangential stiffness matrix of the structure has to be recomputed.

The shell element used here is similar to that developed by Parisch[8] and is based on a nonlinear displacement approach according to

$$\boldsymbol{u} = \boldsymbol{u}_m + \tfrac{1}{2}t\zeta[-\sin\varphi\,\hat{\boldsymbol{e}}_1 + \cos\varphi\sin\theta\,\hat{\boldsymbol{e}}_2 + (\cos\varphi\cos\theta - 1)\hat{\boldsymbol{e}}_3] \tag{2}$$

where $\boldsymbol{u}_m$ is the deformation of the midsurface and $\hat{\boldsymbol{e}}_1$ and $\hat{\boldsymbol{e}}_2$ are orthogonal unit vectors defined in the null space of the shell normal vector $\hat{\boldsymbol{e}}_3$. The normal of the element is assumed to undergo two consecutive rotations $\varphi$ and $\theta$. This formulation is exact for arbitrary translations and rotations of double curved shells in three

Received 7 February 2001; revision received 10 April 2001; accepted for publication 13 April 2001. 

*Ph.D. Student, Department of Aeronautics.

dimensions. For small strains it is possible to use a linear stress-strain relationship in the formulation of the internal forces, which becomes, using index notation,

$$F_{\text{int},k} = \int_{v_e} \frac{\partial \varepsilon_i}{\partial a_k} D_{ij} \varepsilon_j \, \mathrm{d}v \tag{3}$$

assuming summation over $i$ and $j$, where $\varepsilon_i$ is the engineering form of the Green Lagrange strains, $D_{ij}$ is the matrix of elasticity. The tangential stiffness matrix is given by

$$K_{t,kl} = \int_{v_e} \frac{\partial^2 \varepsilon_i}{\partial a_k \partial a_l} D_{ij} \varepsilon_j \, \mathrm{d}v + \int_{v_e} \frac{\partial \varepsilon_i}{\partial a_k} D_{ij} \frac{\partial \varepsilon_j}{\partial a_l} \, \mathrm{d}v \tag{4}$$

again with summation over $i$ and $j$.

## Derivation of String Loads

Assume that a string at one end is attached at an arbitrary point $\boldsymbol{u}_a$ on the structure and that the other end of the string is attached to a fixed point $\boldsymbol{u}_f$ in space. A load is applied to the string so that the resulting force vector becomes

$$\boldsymbol{F}_s = F_s \frac{\boldsymbol{u}_f - \boldsymbol{u}_a}{||\boldsymbol{u}_f - \boldsymbol{u}_a||_2} \tag{5}$$

where $F_s$ is the magnitude of the load. The vector defining the point on the structure can be separated as

$$\boldsymbol{u}_a = \boldsymbol{u}_0 + \boldsymbol{u}_m \tag{6}$$

where $\boldsymbol{u}_0$ is the coordinate of the point when the structure is undeformed. If $\boldsymbol{u}_0$ is the coordinate of a node in the finite element mesh, then $\boldsymbol{u}_m = \boldsymbol{a}_k$. Applying a point load to a finite element structure is not formally correct because it will yield a infinite stress and energy at the point of application. The derivations presented here resemble an approximation of the distributed pressure over the string cross area.

## Experimental Setup and Procedure

The structure investigated is a rectangular, thin plate, as shown in Fig. 1. The plate is made of glass fiber-reinforced epoxy composite with different material characteristics in different directions. Material properties were obtained using acoustic vibration tests on specimens as described in Ref. 9.

The geometric and material properties of the plate are given in Table 1. The plate is clamped between two metal blocks joined with two screws and hangs vertically from the ceiling so that the gravity acceleration vector points along the $y$ axis. The deformations are measured using a three-dimensional optical motion capture system[10] with an absolute error less than 0.05 mm. Half spherical markers are used in order for the cameras to be able to track the markers even for very large deformations. One marker was positioned on the clamping device to investigate the boundary conditions. The results showed no deformation of the clamping device and thus that a clamped boundary condition in the mathematical model should be a good approximation.

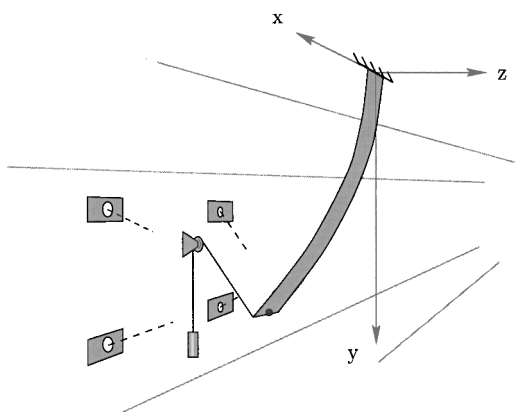


**Fig. 1 Schematic layout of the experimental setup.**

**Table 1 Geometric and material properties**

| Property | Value | Unit |
|---|---|---|
| Semispan | 1.200 | m |
| Chord | 0.150 | m |
| Thickness | 2.960 | mm |
| $E_{11}$ | 25.5 | GPa |
| $E_{22}$ | 23.5 | GPa |
| $E_{12}$ | 3.5 | GPa |
| $E_{21}$ | 3.5 | GPa |
| $G_{12}$ | 5.9 | GPa |
| $G_{21}$ | 3.6 | GPa |
| $G_{31}$ | 4.3 | GPa |
| $\rho$ | 1939.0 | kg/m$^3$ |

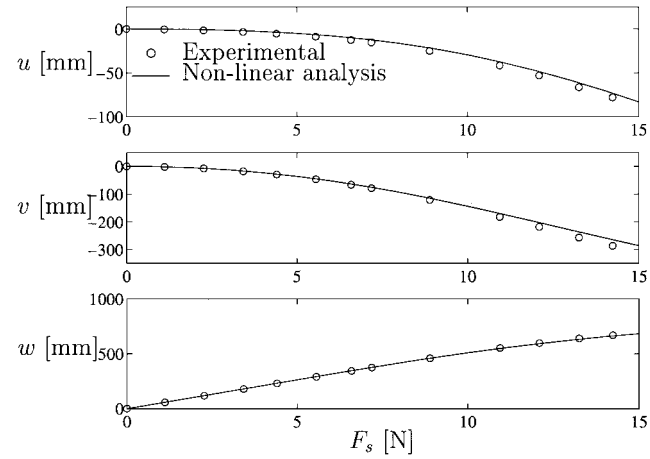


**Fig. 2 Static displacement at marker.**

In the static measurements one end of a thin light string is attached to the plate. The string lies over a low friction wheel with a weight attached to the other end. The wheel is allowed to rotate in the $x$–$z$ plane to dispose side-force effects. A series of measurements for different weights are performed so that displacement as a function of weight can be obtained. For each weight the coordinates of the markers are logged for 5 s using a sampling rate of 240 Hz. The deformations are taken as the mean value of the samples.

In the dynamic measurements the plate was deformed using a weight in the same manner as in the static measurements. Two electrodes were attached to the string close to the plate. A high-voltage current was applied to the electrodes causing the string to burn off almost instantly, minimizing the disturbances caused by the release mechanism. The transient motion was captured for 15 s at a sampling rate of 240 Hz.

## Results

In this section numerical and experimental results are compared and discussed. In the configuration of investigation, the string is attached in the coordinate $(x \;\; y \;\; z) = (0.075 \;\; 1.20 \;\; 0.00)$ and with the wheel located in $(x \;\; y \;\; z) = (-0.22 \;\; 0.68 \;\; 0.87)$, where all values are in meters.

The numerical results were compared to those obtained by Ref. 11, where a cantilever beam is subjected to a suddenly applied pressure load and showed a difference of less then 1% in the maximum amplitude. However, this load case is very hard to model experimentally, and therefore a point load was applied instead.

In Fig. 2 the displacement of the plate at the marker is displayed as a function of the load magnitude $F_s$. The displacement vector is presented as $\boldsymbol{u} = (u \;\; v \;\; w)$. Excellent agreement is obtained between the nonlinear solution and the experimental results.

When comparing experimental and numerical dynamic results, it is important to consider that the equation of motion (1) does not take damping into account. As a consequence of this, the system does

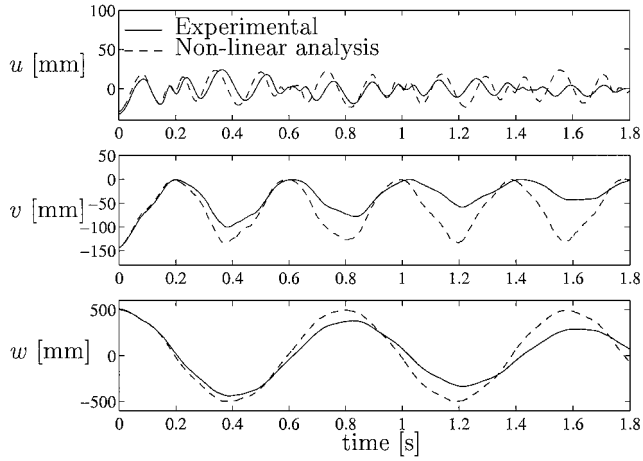


**Fig. 3 Time history deformation at marker.**

not exhibit any loss of energy, and the maximum amplitude of the oscillations does not decrease in time. Furthermore, a system that exhibits damping tends to have a lower frequency than the corresponding undamped system. The experiments presented here were not performed in vacuum but in air, and because of this both aerodynamic and structural damping will contribute to the total damping of the system. However, which one of these that is the dominant part is yet to be investigated.

The initial displacements for the dynamic analysis were obtained from the static solution corresponding to $F_s = 10$ N and coordinates just given. The initial velocities were set to zero. In Fig. 3 numerical results are presented together with experimental.

It is seen that the major characteristics of the oscillations are captured even though no damping is present in the model. However, the difference between the results agree well with the preceding discussion regarding damped vs undamped systems. The computed results show no loss in amplitude and have a slightly higher frequency than the experimental.

## Conclusions

Experimental results of a beamlike plate have been compared to a nonlinear finite element model. Predicted and experimental results for large displacements and rotations in space caused by static loads show excellent agreement. Furthermore, time history dynamic analysis of the moving structure was performed and showed rather good results compared to experimental results even though no damping was present in the model. The three-dimensional nonlinear formulation makes it possible to perform simulation of the transient motion of a structure for arbitrary initial displacements. However, to obtain good agreement for a longer period of time, it is probably necessary to incorporate some type of damping mechanisms in the modeling.

The results of the experiments performed further confirm the use of the optical motion capture system in tracking complex high-frequency motions of simple structures, even for very large displacements.

## Acknowledgments

This work was financially supported by the Swedish Research Council for Engineering Sciences (TFR). The author would like to thank Jakob Kuttenkeuler for guidance and help with the experimental procedures.

## References

[1]Denegri, C., "Limit Cycle Oscillation Flight Tests Results of a Fighter with External Stores," *Journal of Aircraft*, Vol. 37, No. 5, 2000, pp. 761–769.

[2]Bunton, C., and Denegri, C., "Limit Cycle Oscillations Characteristics of Fighter Aircraft," *Journal of Aircraft*, Vol. 37, No. 5, 2000, pp. 916–918.

[3]Patil, D., and Hodges, M., "Nonlinear Aeroelastic Analysis of Complete Aircraft in Subsonic Flow," *Journal of Aircraft*, Vol. 37, No. 5, 2000, pp. 761–769.

[4]Tang, D., Henry, J., and Dowell, E., "Limit Cycle Oscillations of Delta Wing Models in Low Subsonic Flow," *AIAA Journal*, Vol. 37, No. 11, 1999, pp. 1355–1363.

[5]Hughes, T. J. R., Caughey, T. K., and Liu, W. K., "Finite-Element Methods for Nonlinear Elastodynamics Which Conserves Energy," *Journal of Applied Mechanics*, Vol. 45, No. 2, 1978, pp. 366–370.

[6]Gummadi, L. N. B., and Palazotto, A. N., "Nonlinear Dynamic Finite Element Analysis of Composite Cylindrical Shells Considering Large Rotations," *AIAA Journal*, Vol. 37, No. 11, 1999, pp. 1489–1494.

[7]Argyris, H.-P., and Mlejnek, J., *Dynamics of Structures*, Elsevier, Amsterdam, 1991, pp. 478–480.

[8]Parisch, H., "Geometrical Nonlinear Analysis of Shells," *Computer Methods in Applied Mechanics and Engineering*, Vol. 14, No. 2, 1978, pp. 159–178.

[9]Kuttenkeuler, J., "Aircraft Composites and Aeroelastic Tailoring," Ph.D. Dissertation, Rept. 98-13, Dept. of Aeronautics, Royal Inst. of Technology, Stockholm, April 1998.

[10]Kuttenkeuler, J., "Optical Measurements of Flutter Mode Shapes," *Journal of Aircraft*, Vol. 37, No. 5, 2000, pp. 846–849.

[11]Shantaram, D., Owen, D., and Zienkiewicz, D., "Dynamic Transient Behavior of Two- and Three-Dimensional Structures Including Plasticity, Large Deformation Effects and Fluid Interaction," *Earthquake Engineering and Structural Dynamics*, Vol. 4, No. 6, 1976, pp. 561–578.

A. N. Palazotto
*Associate Editor*